International Journal of Bioprinting

RESEARCH ARTICLE

Effect of sterilization processes on alginate/gelatin inks for three-dimensional printing

Teresa Carranza[1,2], Martin Zalba-Balda[3,4], Mari Jose Barriola Baraibar[3], Koro de la Caba[1,5]*, Pedro Guerrero[1,5,6]*

[1]BIOMAT Research Group, University of the Basque Country (UPV/EHU), Escuela de Ingeniería de Gipuzkoa, Plaza de Europa 1, Donostia-San Sebastián, 20018, Spain

[2]Domotek SL, Bº Santa Luzia 17, Tolosa, 20400, Spain

[3]Tknika, Basque VET Applied Research Centre, Barrio Zamalbide s/n, Errenteria, 20100, Spain

[4]University of Mondragon (MU), Faculty of Engineering (MGEP), Loramendi 4, Arrasate-Mondragon, 20500, Spain

[5]BCMaterials, Basque Center for Materials, Applications and Nanostructures, UPV/EHU Science Park, Leioa, 48940, Spain

[6]Proteinmat Materials SL, Avenida de Tolosa 72, Donostia-San Sebastián, 20018, Spain

(This article belongs to the *Special Issue: Advances in the Application of 3D Printing in Medicine and Dentistry*)

Abstract

Sterilization is a crucial step in the process of developing bioinks for tissue engineering applications. In this work, alginate/gelatin inks were subjected to three sterilization methods: ultraviolet (UV) radiation, filtration (FILT), and autoclaving (AUTO). In addition, to simulate the sterilization effect in a real environment, inks were formulated in two different media, specifically, Dulbecco's Modified Eagle's Medium (DMEM) and phosphate-buffered saline (PBS). First, rheological tests were performed to evaluate the flow properties of the inks, and we observed that UV samples showed shear thinning behavior, which was favorable for three-dimensional (3D) printing. Furthermore, the 3D-printed constructs developed with UV inks showed better shape and size fidelity than those obtained with FILT and AUTO. In order to relate this behavior to the material structure, Fourier transform infrared (FTIR) analysis was carried out and the predominant conformation in protein was determined by deconvolution of the amide I band, which confirmed that the prevalence of α-helix structure was greater for UV samples. This work highlights the relevance of sterilization processes, which are essential for biomedical applications, in the research field of bioinks.

Keywords: Inks; Three-dimensional printing; Constructs; Sterilization

†These authors contributed equally to this work.

***Corresponding author:**
Pedro Guerrero (pedromanuel.guerrero@ehu.es)
Koro de la Caba (koro.delacaba@ehu.es)

Citation: Carranza T, Zalba-Balda M, Barriola Baraibar MJ, *et al*., 2023, Effect of sterilization processes on alginate/gelatin inks for three-dimensional printing. *Int J Bioprint*, 9(1): 645
https://doi.org/10.18063/ijb.v9i1.645

Received: July 11, 2022
Accepted: October 11, 2022
Published Online: November 23, 2022

1. Introduction

Many studies have been carried out to address the complexity of tissue engineering in regenerative medicine[1–3]. In this regard, bioprinting technologies, defined as controlled deposition of biological materials to form living structures or structures that will host biological components, called scaffolds, are gaining much attention[4–6]. In this context, it is necessary to approach several perspectives to test the models developed. However,

it is essential to address the safety issue of these printed constructs from the point of view of sterilization, defined as a process that destroys all forms of microbial life, including the bacterial spores[7]. If the elimination of the spores cannot be ensured, the process is considered disinfection, instead of sterilization[7,8].

Two ways are defined to ensure the sterility of final products: (i) final product sterilizations, which occur at the end of the fabrication process and thus is incompatible with works involving cell containing inks[9–11], and (ii) aseptic fabrication processes[12].

Depending on the nature of the sterilizing agent, there are three main types of sterilization, namely physical, chemical, and physicochemical sterilizations[13]. Additionally, physical sterilization is divided into three subtypes, which are the techniques studied in this work: autoclaving, non-ionizing radiation, and filtration[13]. Nevertheless, it should be noted that other techniques, such as ethylene oxide or hydrogen peroxide plasma sterilizations, were not included in this study because of their cost and security requirements[7,8,14–16].

Since cellular load inks are usually prepared with cell culture media, which could modify the properties of fresh inks, the effects of those media should also be considered. For example, Dulbecco's Modified Eagle's Medium (DMEM), a medium used in mammalian cell cultures, contains a small concentration of Ca^{2+}[17], which may interact with some biopolymers, such as alginate, promoting partial crosslinking and inducing a change on rheological properties[17,18].

Nowadays, there is no specific regulation with regard to sterilization of printed biological products, although several pharmacopoeias have begun to focus on this problem[19]. To date, there are few scientific articles that address the influence of sterilization and how this affects the different materials that can be printed[7,13,19–21]. Some sterilization techniques have been proposed and most of them concluded that sterilization techniques should be studied in relation to the material used[7,13,19–21]. In this regard, recent works were focused on the assessment of sterilization methods on gelatin methacryloyl (GelMA) and alginate inks[21,22]. Furthermore, some studies have analyzed the effect of the treatment duration on rheological and physicochemical properties of alginate inks, concluding that shorter autoclave cycles have smaller influence on the original inks[23]. In this work, a mixture of two biopolymers, gelatin and alginate, was used to prepare the ink for three-dimensional (3D) printing. On the one hand, gelatin is a natural protein derived from the hydrolysis of collagen and it is widely used because of its non-toxicity and biodegradability[24]. Gelatin is mainly based on glycine, proline, and alanine and has polyampholytes nature. It is widely used in combination with other polymers, such as alginate and methylcellulose, as well as with cross-linking agents, such as genipin or glutaraldehyde[24,25]. On the other hand, alginate is a polysaccharide derived from brown algae and is a widely used biopolymer in biomedical science due to its ability to form hydrogels via chemical crosslinking with carboxyl and hydroxyl groups and divalent cations[24,26].

While some authors have reported sterilizing acellular constructs by ultraviolet (UV) light and ethanol baths[27,28], little has been reported on the sterilization of inks with the potential to encapsulate cells. Therefore, the aim of this work is to assess the effect of the commonly used sterilization techniques, such as autoclaving[29,30], filtration[31,32], and UV exposure[33,34], on both the inks and the 3D-printed constructs.

In this work, different sterilization methods and different media were evaluated with inks prepared with gelatin and sodium alginate (SA). It is worth highlighting that little has been reported on the sterilization of inks and sometimes the sterilization process used was not even mentioned. This work focuses on investigating the effect of sterilization on the rheological behavior of inks, an important factor that influences the stability and final properties of 3D-printed construct. In order to select the 3D printing parameters, rheological analysis was carried out, and the 3D-printed constructs were analyzed by Fourier transform infrared (FTIR) analysis to determine the effect of the sterilization method and media employed.

2. Materials and methods

2.1. Materials

Gelatin (GEL; type A, bloom 300) and SA from brown algae were purchased from Sigma-Aldrich (Madrid, Spain). Dulbecco's Modified Eagle's Medium (DMEM), GlutaMAX (Gibco™ F12-GlutaMax™ supplemented) and phosphate-buffered saline (PBS) were purchased from Thermo Fisher (Madrid, Spain).

2.2. Sample preparation

Solutions with 7 wt % SA and 8 wt % GEL were prepared at 50°C under magnetic stirring for all the sterilization methods and culture media under study. Three sterilization methods (autoclaving, UV radiation, and filtration) and three media (DMEM, PBS, and water as control) were compared. Water was used as a control to assess the effect of the electrolytes present in the culture media. Autoclaved (AUTO) samples were dissolved in different media and then autoclaved (Selecta, ST DRY PV III 25) at 121°C and

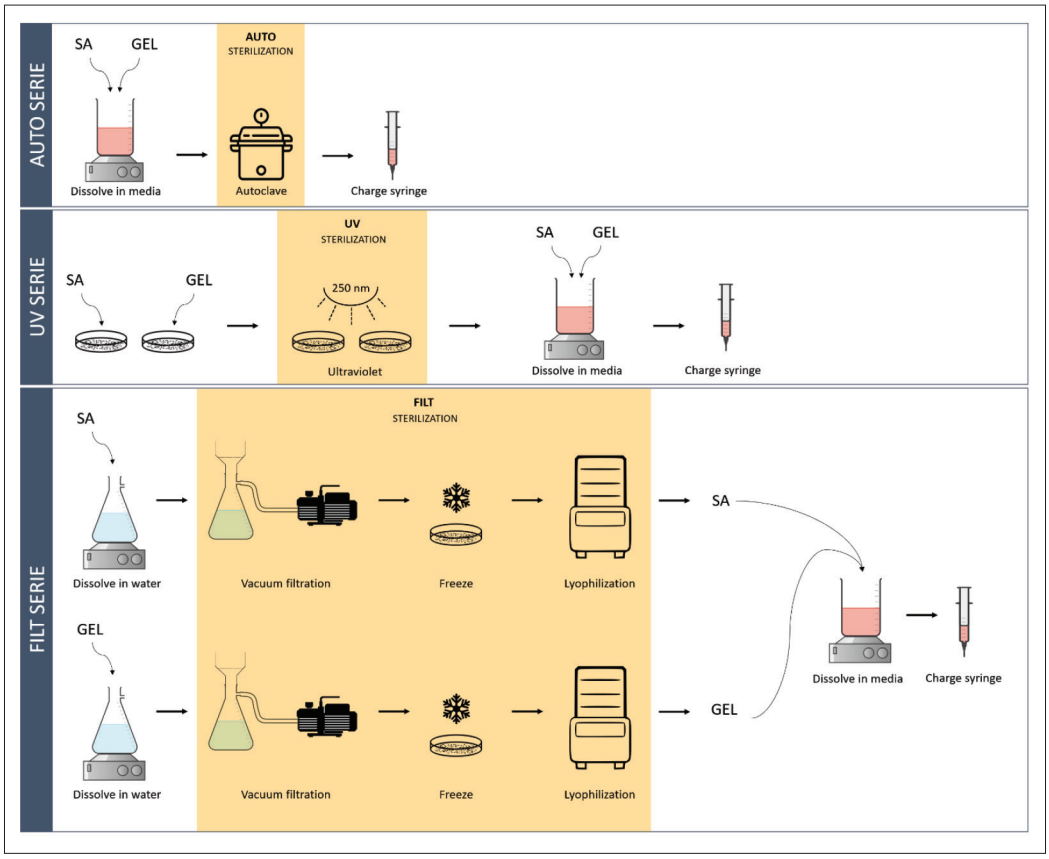

Figure 1. Overview of the studied sterilization techniques.

1 atm for 30 min. To prepare UV-sterilized samples, both GEL and alginate were placed in petri dishes, subjected to 254 nm UV light in a cabinet (MSC-Advantage™) under type-II laminar flow for 30 min, and then were dissolved in sterile cell media. To prepare filtered (FILT) samples, first, both GEL and alginate were dissolved separately at a concentration of 2 wt % in Milli-Q water to prevent filter clogging and passed through 0.22 µm PES vacuum filter. It is worth noting that no supernatant was observed during the filtration process. The resulting filtered solutions were lyophilized to obtain sterilized SA and GEL powders. After that, the same concentrations (7 wt % SA and 8 wt % GEL) were used, as did for the other treatments under study. Non-sterilized solutions were used as control (CONTROL). These sterilization processes are shown schematically in Figure 1.

2.3. Rheological evaluation

Rheological experiments were performed by a Thermo Scientific Haake Rheostress1 Rheometer (IFI S.L., Spain). All tests were set at 37°C and were repeated twice to ensure data reproducibility. One hertz constant frequency and shear rate from 1 s^{-1} to 100 s^{-1} were used to obtain shear viscosity curves, which were fitted to Cross model for shear thinning fluids (Equation I)[35,36]:

$$\eta = \eta_{\infty} + \frac{\eta_0 - \eta_{\infty}}{1 + (C\dot{\gamma})^m} \quad \text{(I)}$$

where η is the viscosity, η_0 and η_{∞} are the viscosities at low and high shear values (zero and infinite shear values), respectively, C is the consistency or cross time constant, $\dot{\gamma}$ is the shear rate, and m is a dimensionless cross rate constant, which is calculated by curve fitting in the slope region.

Shear values in the nozzle wall for each printing conditions were calculated using Weissenberg-Rabinowitsch-Mooney equation (Equation II)[37–39]:

$$\dot{\gamma}_w = \frac{4Q}{\pi r^3}\left(\frac{3n+1}{4n}\right) \quad \text{(II)}$$

where Q is the volumetric flow rate, r is the radius of the tip, and n is the power law index or flow index.

Volumetric flow values were obtained considering filament length (equivalent diameter for 10 mL syringe) and printing time given by Cura 4.13.0 slicing software (Ultimaker, Nederland). Power law index was calculated

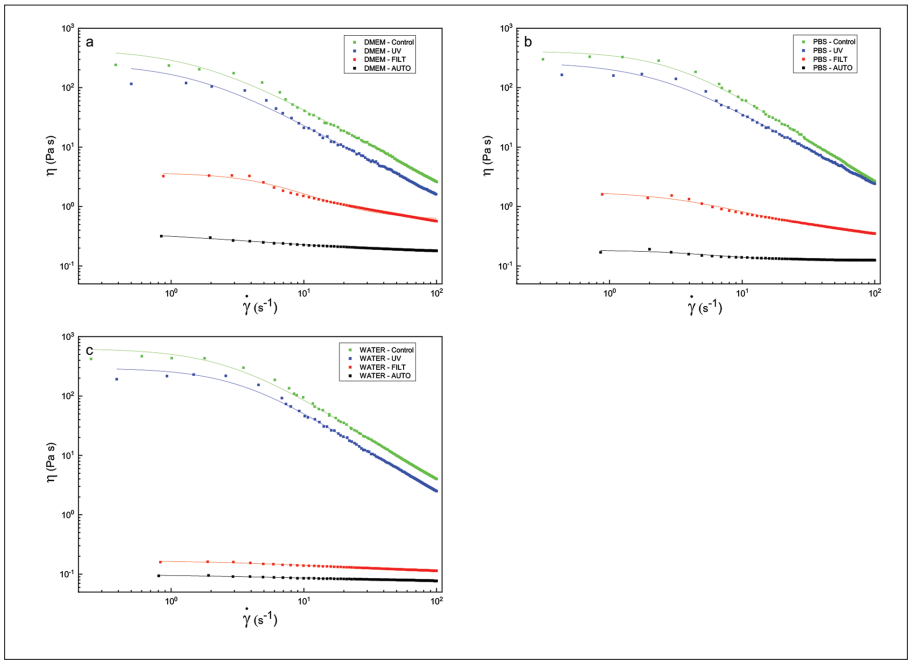

Figure 2. Shear viscosity curves fitted to Cross model (represented by lines) for GEL-SA samples as a function of the sterilization method (CONTROL, UV, FILT, and AUTO) in different media: (A) DMEM, (B) PBS, and (C) water.

assuming the slope of fitted curve (*-m*) as a power law region (*n–1*).

To obtain storage modulus (G'), loss modulus (G'') and loss tangent (tanδ), frequency sweeps were carried out from 0.05 to 100 Hz.

2.4. 3D printing

DomoBIO 2A bioprinter (Domotek, Spain) equipped with heated syringe extruder and refrigerated platform was used for printing tests. The structure was designed with Solid Edge Student (Siemens, Germany). Printed scaffolds had cylinder shape with a diameter of 21 mm and a height of 0.6 mm. Cura 4.13.0 slicing software (Ultimaker, Netherlands) was used for slicing the object. All samples were loaded into 10 mL plastic syringes and heated at 35°C for 30 min before use. 3D printing was carried out at 37°C with 27 G (0.41 mm) conical plastic nozzles, and glass slides were used as deposition substrates. Layer height, layer width, infill line distance, and printing velocity were set up at 0.1 mm, 0.3 mm, 1.5 mm, and 30 mm/s, respectively. Platform temperature and flow index were optimized for each sample in order to improve the dimensional stability of the 3D-printed constructs.

2.5. Fourier transform infrared spectroscopy

FTIR spectra were achieved using a Bruker Alpha-II FTIR spectrometer (Bruker, Spain), equipped with platinum-ATR. A total of 32 scans were performed at 4 cm^{-1} resolution, and all the samples were analyzed in the spectral range of 4000–500 cm^{-1}. Tests were repeated twice to ensure data reproducibility. To obtain second derivative spectra of amide I, data were smoothed using Savitzky-Golay function, and curve fitting was performed via peak analysis using OriginPro 2021 software.

3. Results

3.1. Rheological Evaluation

Rheological properties of hydrogels are one of the most important physical parameters to determine their printability[30,40]. As shown in Figure 2, non-sterilized solutions exhibited shear thinning behavior in all media, since the viscosity decreased with shear rate[41]. However, sterilization processes influenced the rheological behavior of the solutions. It is worth noting that non-sterilized and UV-sterilized samples showed a similar behavior with a marked decrease of viscosity with shear rate. In contrast, this decrease was less noticeable for FILT and AUTO samples, especially when the media was water, in which FILT and AUTO samples showed a Newtonian behavior. Regarding the media employed, the differences observed with water could be due to the presence of inorganic salts in both DMEM and PBS media, which could lead to crosslinking with calcium ions[42–44]. This phenomenon was not observed in FILT and AUTO sterilized samples probably due to the decrease in molecular weight caused by the sterilization treatment[21].

As can be seen in Figure 2, shear viscosity curves were well-fitted to Cross model, and this model parameters are

Table 1. The parameters of Cross model for GEL-SA samples as a function of the sterilization method (CONTROL, UV, FILT, and AUTO) and media (DMEM, PBS, and water) used.

Sample	η_0 (Pa·s)	η_∞ (Pa·s)	C (s)	m	R^2
DMEM-CONTROL	446.79	0.00	0.617	1.244	0.99
DMEM-UV	255.72	0.37	0.619	1.277	0.99
DMEM-FILT	3.70	0.60	0.153	1.611	0.99
DMEM-AUTO	0.42	0.16	0.555	0.617	1.00
PBS-CONTROL	412.19	0.00	0.321	1.468	0.99
PBS-UV	268.80	0.45	0.430	1.299	0.99
PBS-FILT	1.81	0.32	0.178	1.186	1.00
PBS-AUTO	0.18	0.13	0.197	1.639	1.00
Water-CONTROL	629.57	0.00	0.377	1.406	0.99
Water-UV	295.98	0.64	0.297	1.475	0.99
Water-FILT	0.17	0.10	0.075	0.773	1.00
Water-AUTO	0.10	0.07	0.104	0.471	1.00

CONTROL: non-sterilized inks; UV: UV-sterilized inks; FILT: filtered inks; AUTO: autoclaved inks

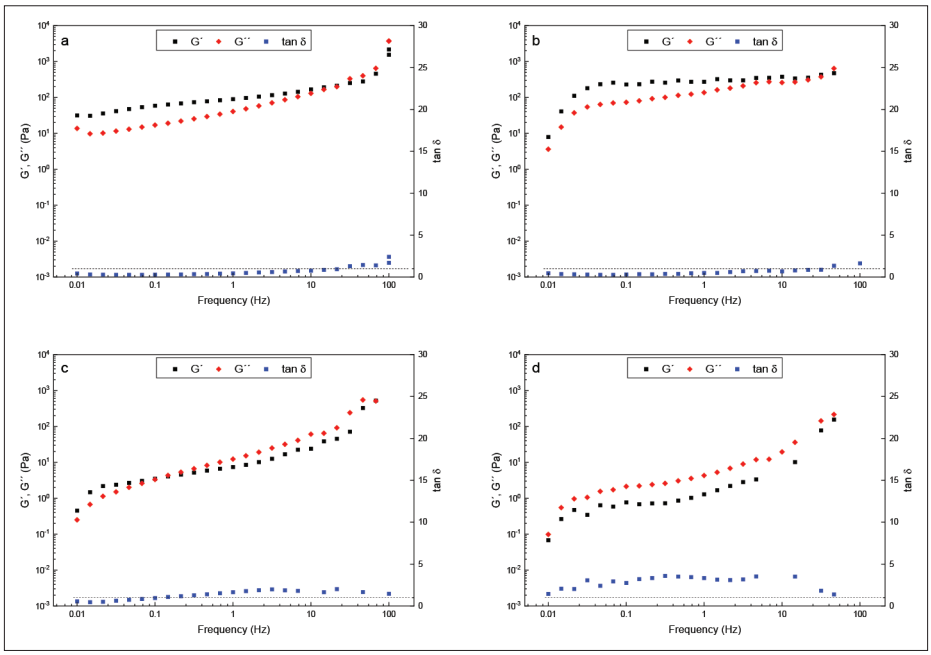

Figure 3. Storage modulus (G'), loss modulus (G") and loss tangent (tanδ) as a function of frequency for: (A) non-sterilized (CONTROL), (B) UV-sterilized (UV), (C) filtered (FILT), and (D) autoclaved (AUTO) GEL-SA samples in DMEM media.

set out in Table 1. All samples, except AUTO and water-FILT samples, demonstrated shear thinning behavior, as evidenced by the difference between μ_0 and μ_∞ values, which showed a drop in viscosity, especially for the DMEM-CONTROL sample. This shear thinning behavior is desirable for 3D-printing applications since viscosity will decrease when shear rate increases during extrusion and thus, sample could be extruded[44–46]. In contrast, no relevant difference was found for AUTO samples in DMEM, PBS, and water media. The Cross time constant (C) and Cross rate constant (m) values, which determine the shear rate in the nozzle ($\dot{\gamma}_w$), are also listed in Table 1.

In addition, frequency sweeps were carried out to determine storage (G') and loss (G") moduli, as well as loss tangent (tanδ), and the resulting curves are shown in Figures 3–5. As can be seen, non-sterilized and UV-sterilized samples (graphs a and b) showed elastic behavior since the values of G' are higher than those of G", regardless of the media used; in contrast, FILT and AUTO samples showed

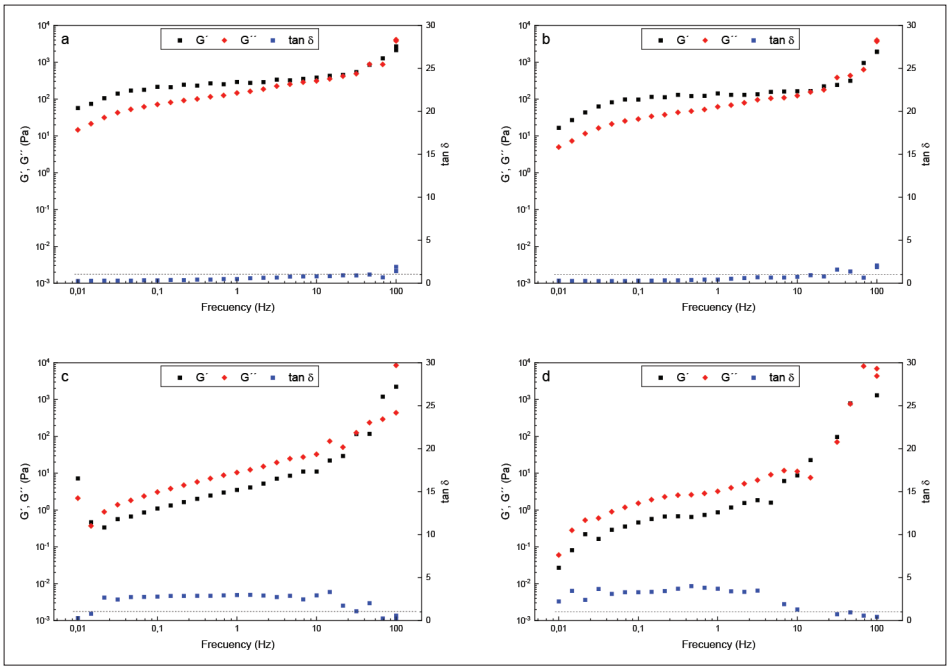

Figure 4. Storage modulus (G'), loss modulus (G") and loss tangent (tanδ) as a function of frequency for: (A) non-sterilized (CONTROL), (B) UV-sterilized (UV), (C) filtered (FILT), and (D) autoclaved (AUTO) GEL-SA samples in PBS media.

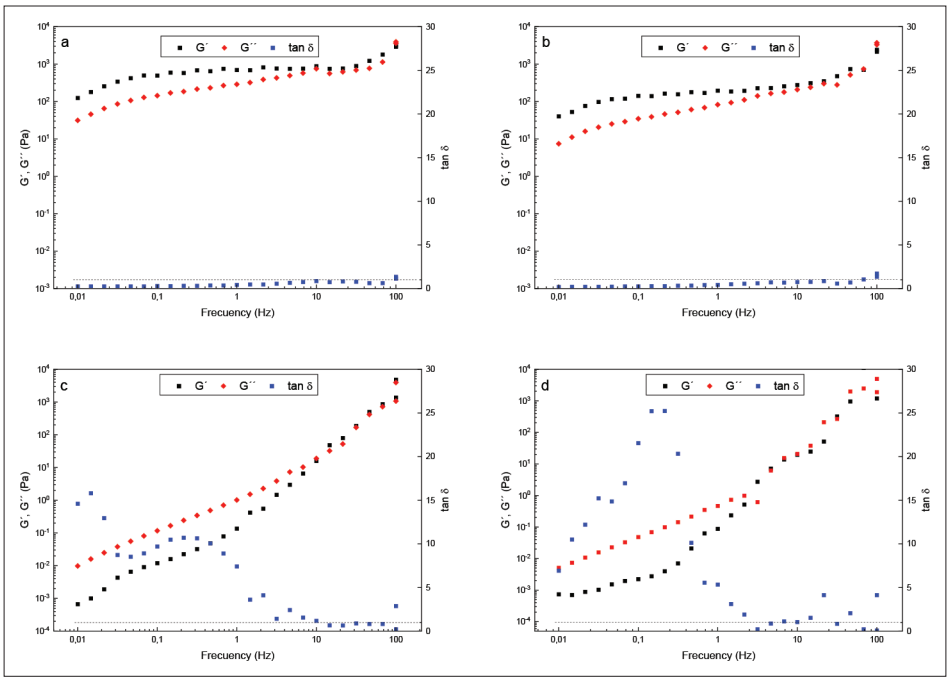

Figure 5. Storage modulus (G'), loss modulus (G") and loss tangent (tanδ) as a function of frequency for: (A) non-sterilized (CONTROL), (B) UV-sterilized (UV), (C) filtered (FILT), and (D) autoclaved (AUTO) GEL-SA samples in water.

viscous behavior (G" > G')[36]. Regarding tanδ values, in almost the entire range of frequency studied, tanδ was lower than 1 for CONTROL and UV samples, indicating a solid-like behavior, while fluid-like behavior (tanδ > 1) was observed in AUTO and FILT samples. Since dimensional stability is essential to form the construct when the ink is deposited on the 3D printer platform, solid-like behavior is required to avoid the collapse of the 3D-printed construct[47].

3.2. 3D printing

The temperature used in the extruder was 37°C for all samples, but the temperature of the 3D printer platform ($T_{platform}$) and flow values (Q) were optimized for each sample. These values, together with the shear rate values in the nozzle section ($\dot{\gamma}_w$), are summarized in Table 2. It was observed that UV samples required the highest platform temperature (18°C) and volumetric flow rate (1.96 mm^3/s), regardless of the media employed. In contrast, AUTO samples needed the lowest platform temperature (12°C) and flow values, regardless of the media used. However, the behavior of FILT samples was dependent on the media, requiring higher temperature and flow rate in PBS media.

Although FILT and AUTO samples were printed precisely for the initial two to three layers, failure started from this point onward. As shown in Figure 6, the accuracy of the constructs obtained with AUTO and FILT samples was not good, with material accumulation and poor definition; pores were collapsed, and significant differences were seen between the theoretical design and the resulting construct (**Figure S1**). It is believed that this behavior after the deposition of the first layers is due to the fact that the effect of the cold temperature on the platform cannot be transmitted to a great number of layers and thus, the heat cannot be dissipated properly and failure occurred[48]. The behavior was similar in the two media tested, DMEM and PBS, with a better definition for the constructs developed with GEL-SA samples in PBS. It is worth noting that UV-cured samples resulted in constructs with a good accuracy and shape fidelity, as can be observed in Figure 6c and f.

Table 2. Printing parameters for GEL-SA samples as a function of the sterilization method (UV, FILT, and AUTO) and media (DMEM and PBS) used.

Sample	$T_{platform}$ (°C)	Q (mm^3/s)	$\dot{\gamma}_w$ (s^{-1})
DMEM-UV	18	1.96	11909
DMEM-FILT	15	1.87	3931
DMEM-AUTO	12	1.83	2416
PBS-UV	18	1.96	3962
PBS-FILT	18	1.90	5072
PBS-AUTO	12	1.83	2660

$T_{platform}$, 3D printer platform temperature; Q, volumetric flow rate; $\dot{\gamma}_w$, shear rate in the nozzle.
CONTROL: non-sterilized inks; UV: UV-sterilized inks; FILT: filtered inks; AUTO: autoclaved inks

3.3. Fourier transform infrared (FTIR) spectroscopy

The constructs were analyzed by FTIR and spectra are shown in Figure 7. A broad band was observed at 3500–3000 cm^{-1}, related to O-H bonds present in both GEL and alginate. Additionally, the characteristic bands of GEL appeared at 1650 cm^{-1} (amide I), corresponding to C=O; at 1560 cm^{-1} (amide II), associated with N-H bending; and at 1240 cm^{-1}, corresponding to C-N stretching. Regarding alginate, the most representative bands appeared at 1093 and 1032 cm^{-1}, corresponding to C-O-C stretching vibrations[49,50]. The most significant changes occurred in relation to the bands corresponding to amide I and II. In general, the relative intensity between these two bands was similar; however, amide II band became less intense for PBS-UV, DMEM-CONTROL, and DMEM-UV samples.

In a further analysis, the band corresponding to amide I was deconvoluted in order to determine the predominant

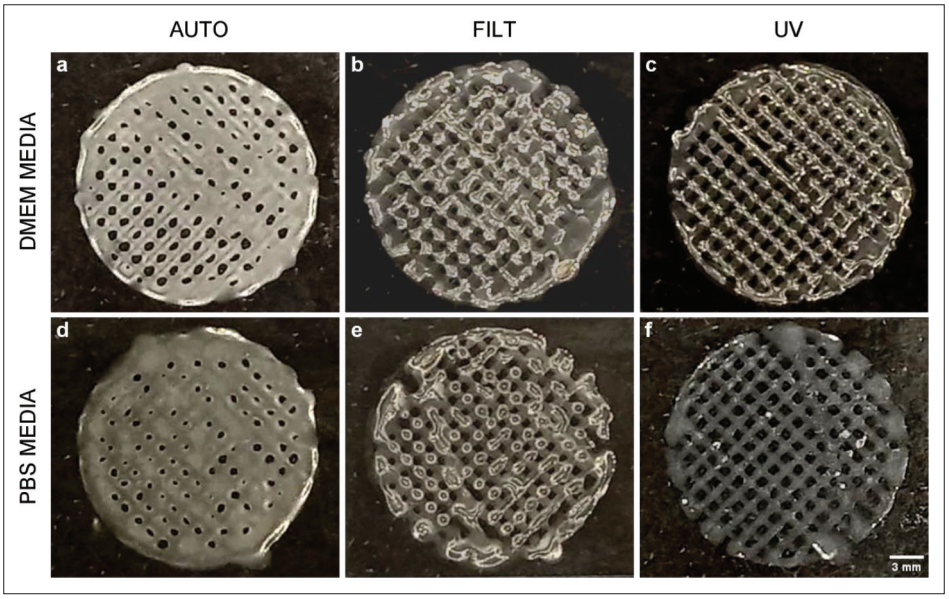

Figure 6. 3D-printed constructs for GEL-SA samples as a function of the sterilization process (AUTO, FILT and UV) and media (DMEM and PBS) used.

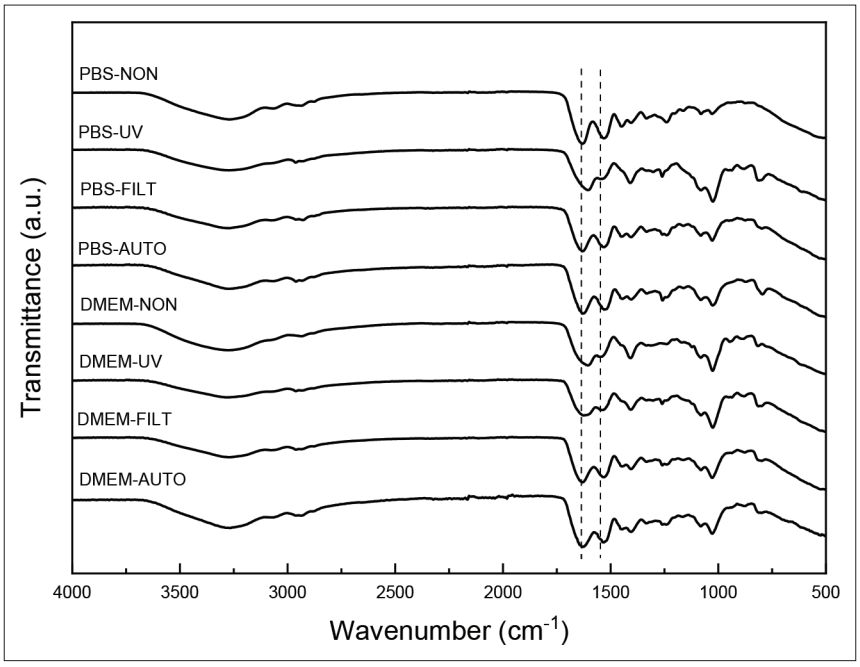

Figure 7. FTIR spectra for GEL-SA samples as a function of sterilization method (CONTROL, UV, FILT, and AUTO) and media (DMEM and PBS) used. Amide I and amide II bands are marked by dotted lines.

Table 3. Secondary structure percentage (%) determined by amide I band deconvolution for GEL-SA samples as a function of sterilization methods (CONTROL, UV, FILT, and AUTO) and media (DMEM and PBS) used.

Protein conformation	DMEM				PBS			
	CONTROL	UV	FILT	AUTO	CONTROL	UV	FILT	AUTO
β-sheet[a]	39.9	41.7	47.6	47.3	51.4	49.3	55.3	52.8
α-helix and random coil	36.7	36.5	31.6	30.5	31.2	30.5	25.2	25.7
β-turns	18.8	17.1	15.3	17.1	13.6	16.8	17.3	16.9
β-sheet[b]	4.6	4.7	5.5	5.1	3.8	3.4	4.2	4.6

[a]Inter-antiparallel and intra-parallel; [b]intra-antiparallel.
CONTROL: non-sterilized inks; UV: UV-sterilized inks; FILT: filtered inks; AUTO: autoclaved inks

secondary structure in GEL[51]. Amide I region contains many different vibrational frequencies in function of secondary structures: intra-parallel and inter-antiparallel β-sheet (1610–1642 cm^{-1}), random coil and α-helix (1645-1660 cm^{-1}), β-turn (1660-1686 cm^{-1}), and intra antiparallel β-sheet (1674–1695 cm^{-1})[51–53]. As can be seen in Table 3, β-sheet conformation was predominant in PBS, while this conformation was predominant only for FILT and AUTO samples in DMEM media. Regarding the sterilization processes, the prevalence of α-helix structure was greater for CONTROL and UV samples. This is in accordance with a higher dimensional stability, as found in UV samples and shown in Figure 7.

These differences in protein conformations may be due to a partial denaturation of the protein, probably due to the conditions used in FILT and AUTO sterilization processes[54]. Once the protein is unfolded, new bonds, with the small inorganic molecules dissolved in the media or with alginate, can be formed, leading to changes in protein secondary structure and therefore, to different flow behavior, as shown by rheological results.

4. Conclusion

Rheological results showed that sterilization processes change the rheological behavior of protein-based inks. While AUTO samples in all media and FILT samples in water behaved as Newtonian fluids, UV samples showed shear thinning behavior, which was favorable for 3D-printing processes. These differences in the rheological properties of the inks were evidenced in the 3D-printing process. In particular, the samples sterilized by UV radiation were the ones with the best preserved shape and size once they were deposited on the 3D printer platform. These results were related to the changes

observed by FTIR analysis; specifically, amide I analysis reported the evidence of the influence of different types of sterilization treatments on the protein secondary structure, with a greater prevalence of the a-helix structure for UV inks. The current study has shown the influence of sterilization processes and media on the rheological behavior of inks. A lattice structure was used to assess the stability of the ink for 3D bioprinting. Future works will focus on investigating the physicochemical properties of the 3D-printed constructs, the efficiency of sterilization processes using microbial testing, and cell encapsulation study on the sterilized ink.

Acknowledgments

None.

Funding

Authors thank Basque Government (IT1658-22 and KK2022-00019) for the funding. T.C. also thanks Basque Government for her fellowship (PRE_2021_1_0254).

Conflict of interest

The authors declare no conflicts of interest.

Author contributions

Conceptualization: Teresa Carranza, Pedro Guerrero
Formal analysis: Teresa Carranza, Martin Zalba-Balda
Funding acquisition: Koro de la Caba
Investigation: Teresa Carranza, Martin Zalba-Balda
Methodology: Mari Jose Barriola Baraibar
Project administration: Koro de la Caba, Pedro Guerrero
Resources: Mari Jose Barriola Baraibar, Koro de la Caba
Supervision: Koro de la Caba, Pedro Guerrero
Writing – original draft: Teresa Carranza
Writing – review & editing: Koro de la Caba, Pedro Guerrero

Ethics approval and consent to participate

Not applicable.

Consent for publication

Not applicable.

Availability of data

Not applicable.

References

1. Lopes Nalesso PR, Wang W, Hou Y, *et al.*, 2021, In vivo investigation of 3D printed polycaprolactone/graphene electro-active bone scaffolds. *Bioprinting*, 24: e00164.
2. Liu X, Xu M, Li P, *et al.*, 2021, Implantation and repair of 3D printed myocardial patch in rabbit model of myocardial infarction. *Bioprinting*, 24: e00165.
3. Maxson EL, Young MD, Noble C, *et al.*, 2019, In vivo remodeling of a 3D-Bioprinted tissue engineered heart valve scaffold. *Bioprinting*, 16: e00059.
4. Tian S, Zhao H, Lewinski N, 2021, Key parameters and applications of extrusion-based bioprinting. *Bioprinting*, 23: e00156.
5. Dutta SD, Hexiu J, Patel DK, *et al.*, 2021, 3D-printed bioactive and biodegradable hydrogel scaffolds of alginate/gelatin/cellulose nanocrystals for tissue engineering. *Int J Biol Macromol*, 167: 644–658.
6. He Y, Yang F, Zhao H, *et al.*, 2016, Research on the printability of hydrogels in 3D bioprinting. *Sci Rep*, 6: 29977.
7. Horakova J, Klicova M, Erben J, *et al.*, 2020, Impact of various sterilization and disinfection techniques on electrospun poly-ε-caprolactone. *ACS Omega*, 5: 8885–8892.
8. Dai Z, Ronholm J, Tian Y, *et al.*, 2016, Sterilization techniques for biodegradable scaffolds in tissue engineering applications. *J Tissue Eng*, 7: 2041731416648810.
9. Stoppel WL, White JC, Horava SD, *et al.*, 2014, Terminal sterilization of alginate hydrogels: Efficacy and impact on mechanical properties. *J Biomed Mater Res B Appl Biomater*, 102: 877–884.
10. Fidalgo C, Iop L, Sciro M, *et al.*, 2018, A sterilization method for decellularized xenogeneic cardiovascular scaffolds. *Acta Biomater*, 67: 282–294.
11. Hofmann S, Stok KS, Kohler T, *et al.*, 2014, Effect of sterilization on structural and material properties of 3-D silk fibroin scaffolds. *Acta Biomater*, 10: 308–317.
12. Munarin F, Bozzini S, Visai L, *et al.*, 2013, Sterilization treatments on polysaccharides: Effects and side effects on pectin. *Food Hydrocoll*, 31: 74–84.
13. Galante R, Pinto TJA, Colaço R, *et al.*, 2018, Sterilization of hydrogels for biomedical applications: A review. *J Biomed Mater Res B Appl Biomater,* 106: 2472–2492.
14. Ribeiro N, Soares GC, Santos-Rosales V, *et al.*, 2020, A new era for sterilization based on supercritical CO2 technology. *J Biomed Mater Res B Appl Biomater*, 108: 399–428.
15. Di Foggia M, Corda U, Plescia E, *et al.*, 2010, Effects of sterilisation by high-energy radiation on biomedical poly-(ε-caprolactone)/hydroxyapatite composites. *J Mater Sci: Mater Med*, 21: 1789–97.
16. Bernhardt A, Wehrl M, Paul B, *et al.*, 2015, Improved sterilization of sensitive biomaterials with supercritical carbon dioxide at low temperature. *PLoS ONE*, 10: e0129205.
17. Hoang VT, Stępniewski G, Czarnecka KH, *et al.*, 2019, Optical properties of buffers and cell culture media for optofluidic and sensing applications. *Appl Sci*, 9: 1145.

18. Puertas-Bartolomé M, Włodarczyk-Biegun MK, del Campo A, *et al.*, 2020, 3D printing of a reactive hydrogel bio-ink using a static mixing tool. *Polymers*, 12: 1986.
19. Lorson T, Ruopp M, Nadernezhad A, *et al.*, 2020, Sterilization methods and their influence on physicochemical properties and bioprinting of alginate as a bioink component. *ACS Omega*, 5: 6481–6486.
20. O'Connell CD, Onofrillo C, Duchi S, *et al.*, 2019, Evaluation of sterilisation methods for bio-ink components: Gelatin, gelatin methacryloyl, hyaluronic acid and hyaluronic acid methacryloyl. *Biofabrication*, 11: 035003.
21. Chansoria P, Narayanan LK, Wood M, *et al.*, 2020, Effects of autoclaving, etoh, and uv sterilization on the chemical, mechanical, printability, and biocompatibility characteristics of alginate. *ACS Biomater Sci Eng*, 6: 5191–5201.
22. Rizwan M, Chan SW, Comeau PA, *et al.*, 2020, Effect of sterilization treatment on mechanical properties, biodegradation, bioactivity and printability of GelMA hydrogels. *Biomed Mater*, 15: 065017.
23. Lafuente-Merchan M, Ruiz-Alonso S, Espona-Noguera A, *et al.*, 2021, Development, characterization and sterilisation of Nanocellulose-alginate-(hyaluronic acid)- bioinks and 3D bioprinted scaffolds for tissue engineering. *Mater Sci Eng C*, 126: 112160.
24. Pan T, Song W, Cao X, 2016, 3D bioplotting of gelatin/alginate scaffolds for tissue engineering: influence of crosslinking degree and pore architecture on physicochemical properties. *J Mater Sci Technol*, 32: 889–900.
25. Merk M, Chirikian O, Adlhart C, 2021, 3D PCL/gelatin/genipin nanofiber sponge as scaffold for regenerative medicine. *Materials*, 14: 2006.
26. Li H, Huang C, Jin X, *et al.*, 2018, An electrospun poly(ε-caprolactone) nanocomposite fibrous mat with a high content of hydroxyapatite to promote cell infiltration *RSC Adv*, 8: 25228–25235.
27. Choi DJ, Park SJ, Gu BK, *et al.*, 2018, Effect of the pore size in a 3D bioprinted gelatin scaffold on fibroblast proliferation. *J Ind Eng Chem*, 67: 388–395.
28. Xu J, Fang H, Su Y, *et al.*, 2022, A 3D bioprinted decellularized extracellular matrix/gelatin/quaternized chitosan scaffold assembling with poly(ionic liquid)s for skin tissue engineering. *Int J Biol Macromol*, 220: 1253–1266.
29. Ren P, Wei D, Liang M, *et al.*, 2022, Alginate/gelatin-based hybrid hydrogels with function of injecting and encapsulating cells in situ. *Int J Biol Macromol*, 212: 67–84.
30. Wu Y, Lin Z Y (William), Wenger AC, *et al.*, 2018, 3D bioprinting of liver-mimetic construct with alginate/cellulose nanocrystal hybrid bioink. *Bioprinting*, 9: 1–6.
31. Russell CS, Mostafavi A, Quint JP, *et al.*, 2020, In situ printing of adhesive hydrogel scaffolds for the treatment of skeletal muscle injuries. *ACS Appl Bio Mater*, 3: 1568–1579.
32. Hamid OA, Eltaher HM, Sottile V, *et al.*, 2021, 3D bioprinting of a stem cell-laden, multi-material tubular composite: An approach for spinal cord repair. *Mater Sci Eng C*, 120: 111707.
33. Hooper R, Arish AA, Alejandre RT, *et al.*, 2022, Chaotic printing of hydrogel carriers for human mesenchymal stem cell expansion. *Procedia CIRP*, 110: 236–241.
34. Fayyabakhsh F, Khayat MJ, Leu MC, 2022, 3D-printed gelatin-alginate hydrogel dressings for burn wound healing: A comprehensive study. *Int J Bioprint*, 8. 274–291.
35. Reis DP, Domingues B, Fidalgo C, *et al.*, 2022, Bioinks enriched with ecm components obtained by supercritical extraction. *Biomolecules*, 12: 394.
36. Pössl A, Hartzke D, Schmidts TM, *et al.*, 2021, A targeted rheological bioink development guideline and its systematic correlation with printing behavior. *Biofabrication*, 13: 035021.
37. Calafel I, Aguirresarobe RH, Peñas MI, *et al.*, 2020, Searching for rheological conditions for FFF 3D Printing with PVC based flexible compounds. *Materials*, 13: 178.
38. Han CD, 1976, *Rheology in Polymer Processing*, Academic Press, New York.
39. Sanchez LC, Beatrice C AG, Lotti C, *et al.*, 2019, Rheological approach for an additive manufacturing printer based on material extrusion. *Int J Adv Manuf Technol*, 105: 2403–2414.
40. Bom S, Ribeiro R, Ribeiro HM, *et al.*, 2022, On the progress of hydrogel-based 3D printing: Correlating rheological properties with printing behaviour. *Int J Pharm*, 615: 121506.
41. Amorim PA, d'Ávila MA, Anand R, *et al.*, 2021, Insights on shear rheology of inks for extrusion-based 3D bioprinting. *Bioprinting*, 22: e00129.
42. Naranda J, Bračič M, Vogrin M, *et al.*, 2021, Recent advancements in 3D printing of polysaccharide hydrogels in cartilage tissue engineering. *Materials*, 14: 3977.
43. Dodero A, Vicini S, Alloisio M, *et al.*, 2020, Rheological properties of sodium alginate solutions in the presence of added salt: an application of Kulicke equation. *Rheol Acta*, 59: 365–374.
44. Lee SC, Gillispie G, Prim P, *et al.*, 2020, Physical and chemical factors influencing the printability of hydrogel-based extrusion bioinks. *Chem Rev*, 120: 10834–10886.
45. Habib MA, Khoda B, 2022, Rheological analysis of bio-ink for 3D bio-printing processes. *J Manuf Process*, 76: 708–718.
46. Schwab A, Levato R, D'Este M, *et al.*, 2020, Printability and shape fidelity of bioinks in 3D bioprinting. *Chem Rev*, 120: 11028–11055.
47. Chen H, Fei F, Li X, *et al.*, 2021, A facile, versatile hydrogel bioink for 3D bioprinting benefits long-term subaqueous fidelity, cell viability and proliferation. *Regen Biomater*, 8: rbab026.

48. Gómez-Blanco JC, Mancha-Sánchez E, Marcos AC, *et al.*, 2020, Bioink Temperature influence on shear stress, pressure and velocity using computational simulation. *Processes*, 8: 865.

49. Ke C-J, Chiu K-H, Chen C-Y, *et al.*, 2021, Alginate-gelatin based core-shell capsule enhances the osteogenic potential of human osteoblast-like MG-63 cells. *Materials & Design*, 210: 110109.

50. Steven E, Saleh WR, Lebedev V, *et al.*, 2013, Carbon nanotubes on a spider silk scaffold. *Nat Commun*, 4: 2435.

51. Yang H, Yang S, Kong J, *et al.*, 2015, Obtaining information about protein secondary structures in aqueous solution using Fourier transform IR spectroscopy. *Nat Protoc*, 10: 382–396.

52. Fellows AP, Casford MTL, Davies PB, 2020, Spectral analysis and deconvolution of the amide I band of proteins presenting with high-frequency noise and baseline shifts. *Appl Spectrosc*, 74: 597–615.

53. Ladner-Keay CL, Griffith BJ, Wishart DS, 2014, Shaking alone induces de novo conversion of recombinant prion proteins to β-sheet rich oligomers and fibrils. *PLOS ONE*, 9: e98753.

54. Guerrero P, Garrido T, Garcia-Orue I, *et al.*, 2021, Characterization of bio-inspired electro-conductive soy protein films. *Polymers*, 13: 416.